Article

Structural Stability and Mechanical Analysis of PVC Pipe Jacking under Axial Force

Rudong Wu, Kaixin Liu [ID]**, Peng Zhang *, Cong Zeng, Yong Xu and Jiahao Mei**

Faculty of Engineering, China University of Geosciences, Wuhan 430074, China; rudongwu@cug.edu.cn (R.W.); lkx@cug.edu.cn (K.L.); zengcong@126.com (C.Z.); xyong@cug.edu.cn (Y.X.); meijiahao@cug.edu.cn (J.M.)
* Correspondence: cugpengzhang@cug.edu.cn

Abstract: PVC pipe jacking is prone to cause yielding or buckling under the jacking force and may lead to engineering failure. The relationship between the buckling modes, ultimate bearing capacity, different diameter–thickness ratios, and length–diameter ratios of PVC pipe jacking under different load forms was analyzed. The calculation methods for allowable jacking force and the single allowable jacking distance are obtained through theoretical analysis and three-dimensional finite elements. The buckling mode of the pipe under uniform load changes from symmetric buckling to asymmetric buckling and then to the overall Euler buckling form as the length–diameter ratio increases. The ultimate bearing capacity of the pipe approaches the theoretical value of yield failure when $L/D \leq 6$. For $L/D > 6$, the pipe undergoes buckling, and the ultimate bearing capacity determined by the axial buckling value and the buckling load can be calculated according to the long pipe theory formula when $L/D > 8.5$. Under eccentric loads, the failure mode transitions from local failure to Euler buckling with increasing pipe length. The ultimate bearing capacity of pipe is obviously lower than that of uniform load, but as the length–diameter ratio increases, this difference decreases until it becomes consistent.

Keywords: pipe jacking; structural stability; buckling load; ultimate bearing capacity

1. Introduction

Pipe jacking is an advanced underground pipe-laying technology with less environmental impact [1–4]. Only high-load-bearing pipe materials could be used in the early stages of micro tunnels, such as concrete pipes, fiberglass-reinforced plastic pipes, and steel pipes [5–7]. Although PVC is a high-quality material for water supply and drainage pipes, it is often used for buried pipelines rather than trenchless methods. A low-load-bearing pipe jacking system was developed, allowing PVC to be used in pipe jacking as technology progressed [8,9].

An important factor that limited the use of PVC pipes in micro tunnels was its axial bearing capacity [10,11]. An experimental setup was developed by Jemii et al. [12] to study the circumferential mechanical characteristics of PVC pipes. Furthermore, a finite element model was created to predict the mechanical response of the pipes under radial loads. The stress characteristics of arch-shaped axial hollow wall PVC pipes, as well as the impact of the pipe wall layout form on pipe stiffness and strength performance, were analyzed by Tang et al. [13] based on buried model tests and simulation analysis. The conclusion that the axial hollow wall is structurally preferable with a circular hole configuration was attained. When considering the stability of PVC pipe jacking under axial load during construction, studies on the stability of steel pipe jacking can serve as a reference. The relationship between critical axial pressure for steel pipe jacking and various parameters has been extensively researched by many scholars [14–16]. The theoretical derivation for axially loaded cylindrical shells was conducted by scholars in the early 20th century. Fok [17] used the energy method combined with the Rayleigh–Ritz trial function to analyze the

buckling of long cylindrical shells under far-field hydrostatic pressure. The compressive strain capacity of a pressurized pipeline under eccentric axial compression was numerically studied by Tu [18]. At the same time, the effects of internal pressure and the ratio of pipe diameter to wall thickness on the compressive strain capacity were studied.

Thus far, the current literature has seldom focused on the mechanical characteristics and axial bearing capacity of PVC pipe jacking. Most of the research literature is mainly focused on the circumferential bearing performance of buried pipes and the buckling stability of steel pipe jacking [19–22]. Compared to steel pipes, the strength of PVC pipes is lower, and yield failure or buckling in PVC might be observed when subjected to significant axial pressure. Therefore, a study on the mechanical characteristics of PVC pipe jacking under axial pressure is essential. The relationship between the ultimate bearing capacity and PVC pipes with different lengths and diameters is also important to study, to prevent the failure of the PVC pipe caused by jacking force.

This paper investigates the failure modes and mechanical properties of PVC pipe jacking under axial uniform force and two eccentric loads through theoretical research and numerical simulation. The influence of the diameter–thickness ratio and the length–diameter ratio on the ultimate bearing capacity of PVC pipes are analyzed and compared with theoretical formulas. Furthermore, the elastic buckling load and ultimate bearing capacity of PVC pipes are obtained and, when combined with the study of the bearing capacity of a single PVC pipe, the calculation method for the allowable jacking force and the single allowable jacking distance are derived.

2. Methodology

2.1. Failure Modes under Axial Loads

A low-load one-time construction method is to use PVC pipe for jacking. In this method, the frontal resistance required by the cutter head jacking acts on the spiral rod inside the pipe. The PVC pipe only bears the friction resistance between the surrounding soil and the outer surface of the pipe and is not affected by the head-on resistance. The axial force of the PVC pipe is greatly reduced, and the risk of buckling of the PVC pipe during jacking is also reduced. The force transfer mechanism enables PVC pipe to be applied in pipe jacking engineering. The principle of PVC micro pipe jacking is shown in Figure 1.
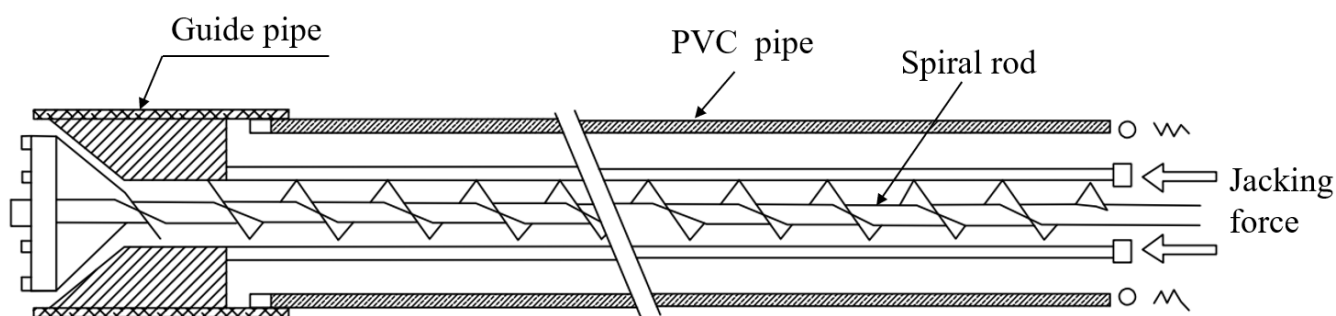
Figure 1. Schematic diagram of PVC pipe jacking principle.

However, although this method can be used to apply PVC pipe to the pipe jacking, it still has the risk of buckling or yield failure under the action of axial force. It is of great significance to clarify the ultimate bearing capacity and buckling modes of PVC pipe under different conditions for pipe jacking construction to determine which type of failure is more likely to occur in PVC pipes under different axial loads. The finite element model of PVC pipe was established by ABAQUS 6.14 software. The shape change energy density theory and cylindrical shell analysis theory were analyzed. The corresponding flow chart of this paper is shown in Figure 2.
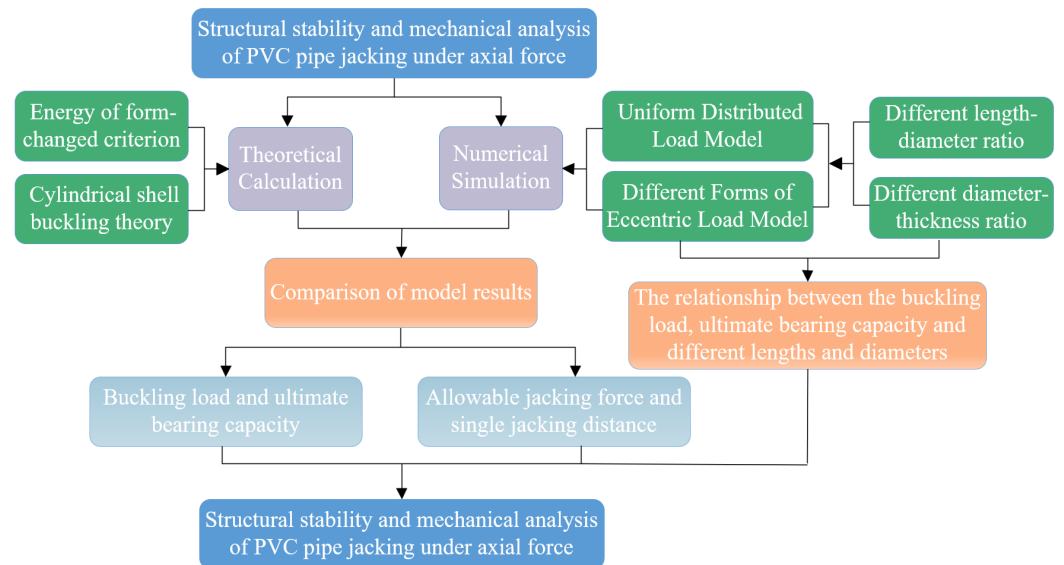
Figure 2. The main research content flow chart of this paper.

(1) Energy of form-changed criterion

The energy of form-changed criterion refers to a strength theory used to determine if a material undergoes yield failure, also known as the fourth yield criterion [23,24]. Yield failure will occur when the shape changes specific energy at a point that reaches the level at which the material yields under the complex state of stress. The formula for strength conditions is shown in Equation (1):

$$\sqrt{\frac{1}{2}\left[(\sigma_1 - \sigma_2)^2 + (\sigma_2 - \sigma_3)^2 + (\sigma_1 - \sigma_3)^2\right]} \leq [\sigma] \tag{1}$$

where σ_1, σ_2, and σ_3 represent the three principal stresses at the critical point of the component in the formula.

For PVC pipes under axial uniform force, yield failure is determined according to Equation (2).

$$P_d = A_p * \sigma_u \tag{2}$$

where A_p is the cross-sectional area of the pipe, m^2, and σ_u is the yield strength of the pipe material, Pa.

(2) Cylindrical shell buckling theory

The failure form of PVC pipe jacking under axial loads can be similar to the buckling of cylindrical shells. The buckling load of axially compressed cylindrical shells is influenced by the length. They are classified into short cylindrical shells [25,26] and long cylindrical shells [27] based on different buckling modes. The buckling load for short cylindrical shells is calculated using Equation (3), while the buckling load for long cylindrical shells is calculated using Equation (4).

$$P_{cr} = \frac{2\pi E t^2}{\sqrt{3(1 - v^2)}} \tag{3}$$

$$P_{cr} = \frac{\pi^3 E D^3 t}{8(\mu_0 l)^2} \tag{4}$$

In the formula, E is the elastic modulus (N/m^2), D is the diameter of the cylindrical shell (m), t is the thickness of the cylindrical shell (m), v is the Poisson ratio, l indicates the length of the cylindrical shell (m), and μ_0 is the effective length factor, which varies depending on boundary conditions.

2.2. Finite Element Model

The finite element models of the PVC pipe were developed using the ABAQUS 6.14 finite element software. To obtain more accurate results of PVC pipe jacking failure modes and bearing capacity, the model was set as follows.

(1) Element and material: The PVC pipe was simulated by a three-dimensional shell element and the elastic-plastic constitutive model was adopted for PVC pipe. According to the experimental research and numerical simulation of previous scholars [12,28,29], the elastic modulus can be taken as 3000 MPa and the compressive yield strength and tensile yield strength are 86.71 MPa and 51.58 MPa, respectively. The finite element model of the PVC pipe is shown in Figure 3, and the pipe parameters are listed in Table 1.
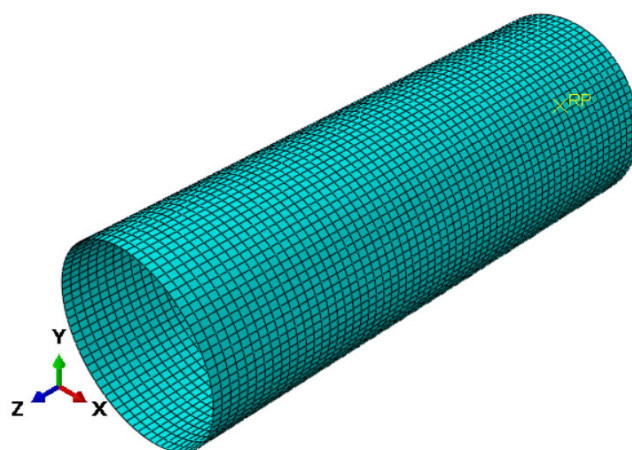
Figure 3. Numerical calculation model for PVC pipes.

Table 1. Pipe parameters of finite element model.

Material	Density (kg/m³)	Diameter (mm)	Wall Thickness (mm)	Pipe Length (m)	Elastic Modulus [28] (MPa)	Compressive Yield Strength [12,28] (MPa)	Tensile Yield Strength [29] (MPa)	Poisson Ratio
PVC Pipe	1360	223.6	11.8	0.6	3000	86.71	51.58	0.319

(2) Element selection and mesh division: The simulation employed three-dimensional shell elements referred to as S4R (four-node reduced integral shell element). S4R has good applicability and can be automatically adjusted between thin and thick shell elements, which can be used for large deformation calculations. The accuracy of the calculation results is greatly affected by the number of elements [30]. To determine the selection of element type and density, many simulations were carried out in this paper. The elastic buckling results of S4R (four-node reduced integral shell element) and S8R (eight-node reduced integral shell element) at the mesh density of 0.01 and 0.005 were compared under method B, as shown in Table 2. The calculation results of the S4R type were closer to the theoretical values, and the mesh density did not change much after 0.01. Therefore, the three-dimensional S4R (four-node reduced integral shell element) was employed and the number of pipe meshes for a 0.6 m length was 4186.

Table 2. The influence of mesh type and density on the results.

| Mesh Type	Mesh Density	Simulated Values (kN)	Theoretical Value (kN)
S4R	0.01	1421	
	0.005	1414	
			1617
S8R	0.01	1337	
	0.005	1389	

(3) Boundary condition and compression load: For the boundary condition setting of the model, one end of the PVC pipe was fixed while the other end was hinged and the two were coupled by the coupling command. The reference points were set at the center of both ends of the shell and the two were coupled by the coupling command, and the boundary conditions were set at these two reference points. The compressive load selects the force load and the displacement load. The force load was applied by applying a concentrated force at the force action or applying a shell edge load at the pressurized end section. The displacement load controls its motion or deformation by applying a vector displacement to the target force.

(4) Simulation methods: The static general analysis step is usually used to calculate the structure with constant or increased structural stiffness in ABAQUS 6.14. If the structure buckles or collapses, it is easy to have non-convergence problems which may prevent it from calculating the post-buckling state. To compare the results of the Buckle–Riks analysis step, two methods were used. The soil layers were not established and the interaction between the pipe and the soil was not considered in the model. Method A: the static general analysis step is selected, the axial pressure is simulated by applying the displacement load to the reference point of the pressure end, and the load-displacement curve is output to determine its bearing capacity. Method B: Buckle–Riks is used to calculate the buckling eigenvalue, and then the defect is introduced to calculate the post-buckling result through the Riks analysis step.

3. Results under Uniform Load

The buckling modes of PVC pipes under uniform axial load obtained using Method A and Method B are shown in Figures 4 and 5, respectively. As shown in Figure 4, the model was compressed in a corrugated manner under the static general analysis step, and the compressive stress on the model was symmetrically distributed. Additionally, the load-analysis step curve in Method A first increased and then decreased. It can be seen from Figure 5 that in Method B, where the Buckle analysis step was used, the five buckling modes of the short pipe exhibited varying deformation patterns.
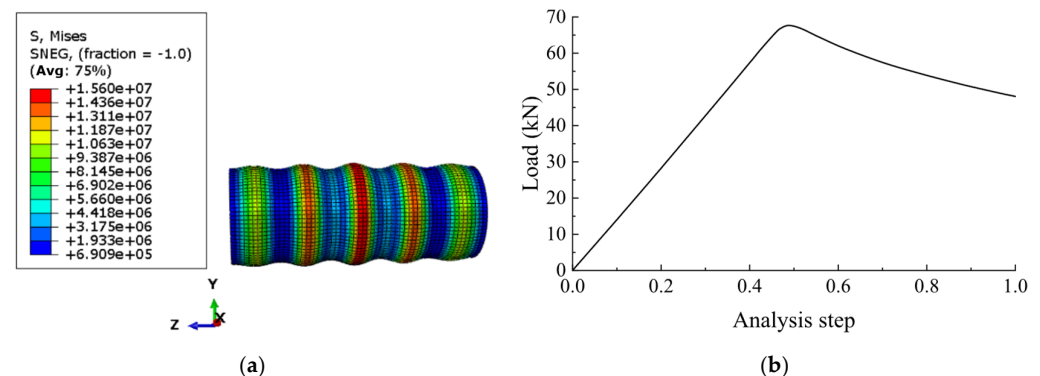
Figure 4. Numerical results of Method A: (**a**) model failure mode; (**b**) load-step curve.

The first two buckling modes showed anti-symmetric buckling for two symmetric points on the pipe; one is convex while the other is concave. The last three buckling modes exhibited symmetric buckling, the number of circumferential waves generated on the pipe gradually decreased, and the peak position appeared in the middle of the pipe. The deformation of the pipeline under axial compression was mainly composed of circumferential deformation and vertical deformation on the cross-section. The buckling mode of the pipeline was greatly affected by the eigenvalue. In the fifth mode, only the middle of the pipe produced a depression. From the first to the fifth mode, the length of the deformed pipe gradually decreased, and the number of deformation waves also decreased. The characteristic values were consistent with the buckling modes.
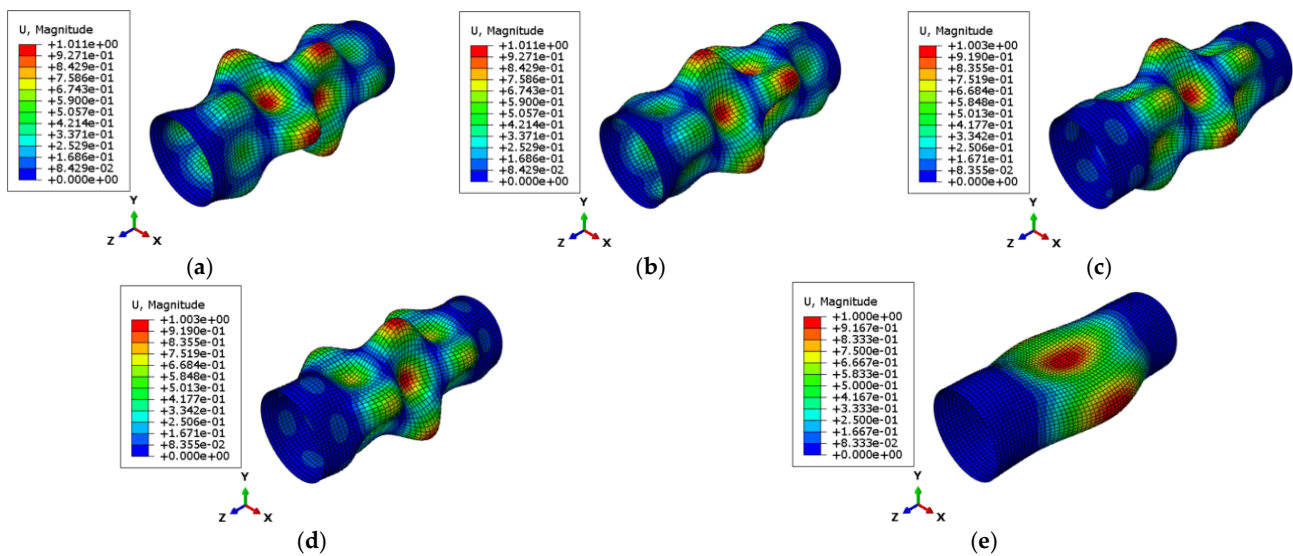
Figure 5. Buckling mode under the Buckle analysis step: (**a**–**e**) eigenvalue of mode 1~eigenvalue of mode 5.

The comparison of results from different theories and two simulation methods is shown in Table 3. The results of simulation Method A were more aligned with the fourth yield criterion, while the results from Method B were closer to the classical critical buckling solution for short pipes. This size of PVC pipe was more likely to experience yield failure first based on the results.

Table 3. Comparison between numerical results and theoretical results.

|	Fourth Yield Criterion	Method A	Short Pipe Theory	Method B
Critical buckling load/kN	683.1	676.4	1617	1421

3.1. Method A Results

The comparison and error between the simulated and theoretical values under different lengths, wall thicknesses, and diameters are shown in Table 4. The error in Table 4 is obtained by 1 minus the simulated value divided by the theoretical value and the error between the two is small, which can correctly reflect the accuracy of the simulation. The changes in the simulated values and theoretical values of the axial bearing capacity of the pipe with length, diameter, and wall thickness are shown in Figure 6. Only the length of the pipe changed; the theoretical value for the PVC pipe's bearing capacity remained constant. This is because the axial bearing capacity of the pipe was not influenced by the pipe length in the fourth yield criterion. The simulation values showed minor variations with changes in pipe length but were generally stable. The curve fluctuations when the pipe was shorter were affected by the boundary conditions.

When the wall thickness and diameter of a PVC pipe increased, its axial bearing capacity also increased, and the two were approximately linearly related. When the wall thickness of the PVC pipe increased from 4.4 mm to 22.3 mm, its bearing capacity rose from 244.93 kN to 1264.49 kN. For every 100 mm increase in the pipe diameter, the bearing capacity increased by about 300 kN. The bearing capacity of pipes under axial uniform force showed strong consistency with the results from yield theory under Method A. Combined with the observed deformation patterns under axial pressure, it mainly reflected the nonlinearity of the material. The simulation results for all three scenarios aligned well with the theoretical values, which also showed the accuracy of the simulation in this paper.

Table 4. Effects of pipe length, diameter, and wall thickness on simulated and theoretical values.

		Simulation Value (kN)	Theoretical Value (kN)	Deviation (%)
Length (m)	0.6	676.4	683.1	0.98
	0.9	685.9	683.1	0.41
	1.2	675.6	683.1	1.09
	2.0	676.2	683.1	1.01
	3.0	674.3	683.1	1.30
Diameter (mm)	223.6	676.4	683.09	0.98
	300	892.26	929.49	4.00
	400	1172.87	1252.01	6.32
	500	1527.97	1547.52	1.26
	600	1787.63	1897.04	5.77
Wall thickness (mm)	4.48	244.93	267.84	8.55
	5.59	320.36	333.09	3.82
	7.45	404	440.13	8.21
	8.94	514	524.51	2.00
	11.95	676.4	683.09	0.98
	14.91	866.96	850.45	1.90
	22.36	1264.49	1229.86	2.74
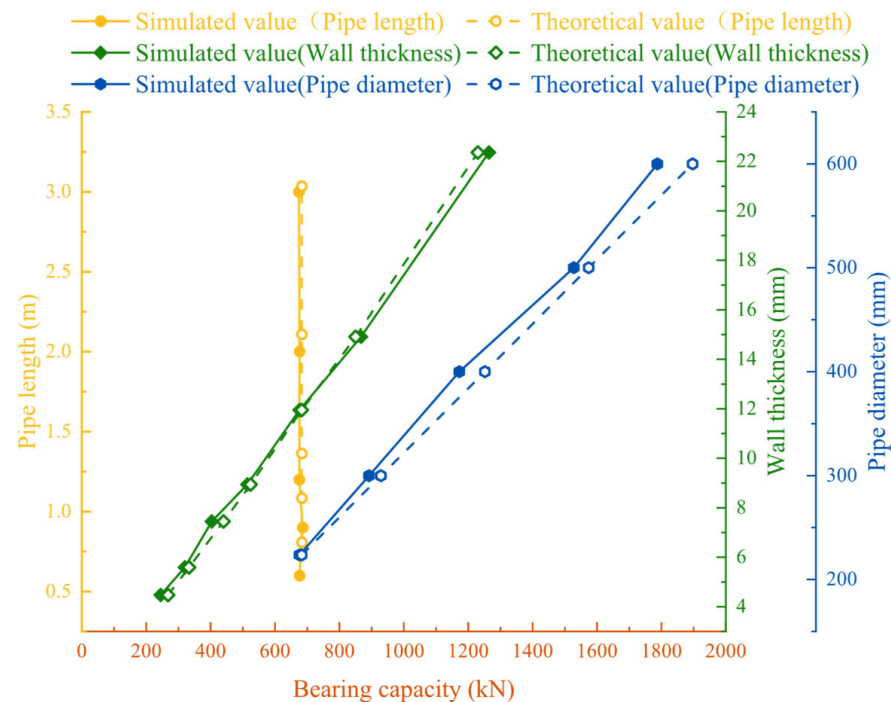
Figure 6. Comparison of theoretical and simulated values for different lengths, wall thicknesses, and diameters.

3.2. Method B Analysis

Elastic theory analysis was conducted on the buckling model. A force was applied to the reference point of the hinged end, and the concentrated force along the axial direction of the pipe was used as the axial uniform force. The length and wall thickness of the pipe were varied. The buckling modes for pipes with L/D ≤ 6, 6 < L/D ≤ 8.5, and L/D > 8.5 are shown in Figure 7. The first mode buckling values under uniform axial load for different sizes of PVC pipes are presented in Table 5. As shown in Figure 7, as the length–diameter ratio increased, the buckling mode of the pipe transitioned from symmetric buckling to anti-symmetric buckling and ultimately to the overall Euler buckling pattern. The number of radial and circumferential waves on the pipe also decreased with an increasing length–diameter ratio.
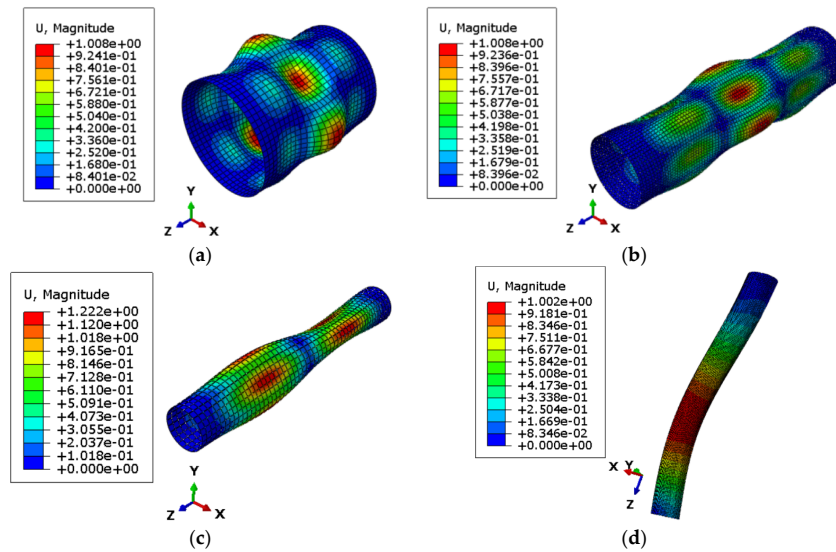
Figure 7. Buckling modes of different lengths: (**a**) 0.3 m; (**b**) 0.9 m; (**c**) 1.6 m; (**d**) 2 m.

Table 5. Elastic buckling values under axial uniform force (kN).

t (mm) \ L (m)	0.3	0.6	1.2	2.0	3.0	7.0
5.59	351.62	341.96	312.41	265.46	148.28	26.89
7.45	612.51	573.59	523.37	409.68	194.41	31
8.94	855.42	804.56	700.95	485.33	230.21	36.65
11.8	1485.95	1421	1138.59	624.64	296.12	47.02
14.91	2274.79	2004.92	1716.59	767.41	363.65	57.60
22.36	4575.95	3892.12	3486.38	1073.37	508.47	80.08

The curve of the elastic buckling load for PVC pipes with different lengths as a function of the diameter–thickness (D/t) ratio is shown in Figure 8a. The curve showing the elastic buckling load for PVC pipes with different wall thicknesses as a function of the length–diameter ratio is plotted in Figure 8b. The buckling load for PVC pipes of various lengths decreased as the D/t ratio increased, and when the D/t ratio was low, the buckling load for shorter PVC pipes was significantly higher than that of longer pipes. When the D/t ratio was 10, the buckling load for a 0.3 m long PVC pipe was about 4575 kN, which is approximately 57 times the buckling load of a 7 m long PVC pipe. As the D/t ratio increased, the effect of length on the buckling load of PVC pipes gradually diminished, eventually tending to be consistent.
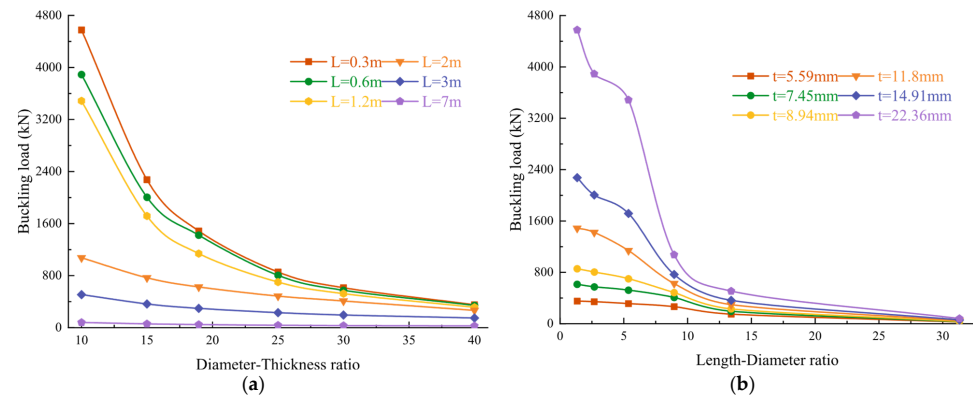

Figure 8. The curve of elastic buckling load as a function of diameter–thickness ratio and length–diameter ratio: (**a**) diameter–thickness ratio; (**b**) length–diameter ratio.

As seen in Figure 8b, the elastic buckling load of the pipe is inversely correlated with the length–diameter (L/D) ratio. At an L/D ratio of 1.34, the wall thickness had the greatest impact on the buckling load. At this ratio, the buckling load for a wall thickness of 22.36 mm was approximately 14.6 times that for a wall thickness of 5.59 mm. However, as the L/D ratio increased, the buckling loads for PVC pipes with different wall thicknesses gradually decreased and converged. The variations in buckling load across different L/D ratios demonstrated a more staged behavior, influenced by the buckling modes.

The comparison of elastic buckling values for PVC pipes under axial uniform force with the short pipe theory is presented in Figure 9a. When the L/D ratio was low, the buckling load of the pipe was close to the results calculated using the short pipe theory. However, this consistency gradually diminished as the L/D ratio increased. When the L/D ratio exceeded 6, a significant deviation occurred, indicating that the short pipe theory was no longer suitable for calculating the buckling load of PVC pipes.
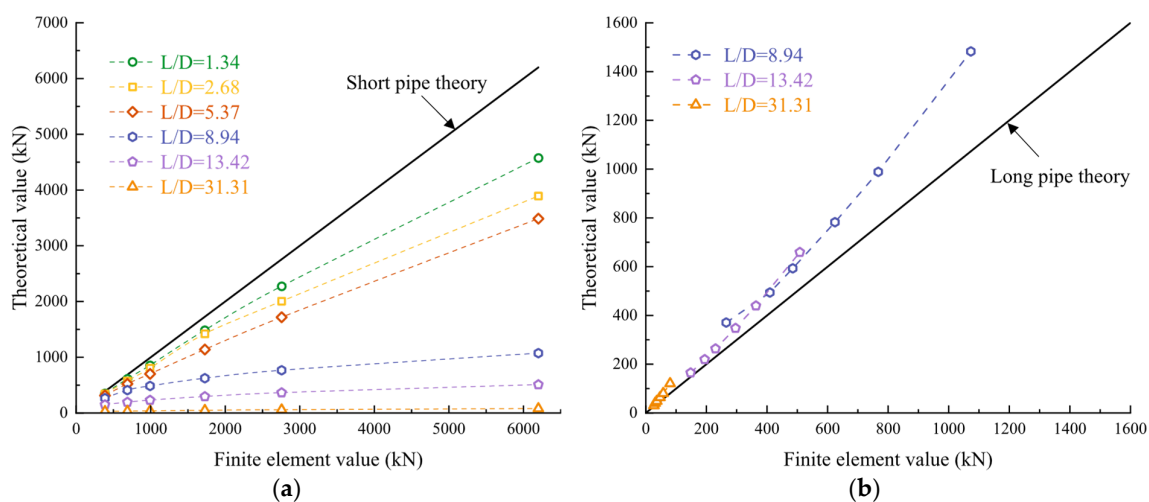
Figure 9. Comparison of finite element results with theoretical values: (**a**) short pipe theory; (**b**) long pipe theory.

Figure 9b plots a comparison between the elastic buckling loads for PVC pipes with an L/D ratio greater than 8.5 and the long pipe theoretical formula. As shown in Figure 9b, when L/D > 8.5, the results for elastic buckling load aligned well with the long pipe theoretical formula. Consequently, under axial uniform force, buckling loads were close to the short pipe theoretical formula when L/D was approximately 6 and converged toward the long pipe theoretical formula when L/D was around 8.5.

The results reflect elastic bearing capacity; the post-buckling stage was not considered. The first buckling mode was introduced into the pipe model as an initial imperfection to analyze post-buckling. The first-order axial buckling mode was scaled by a certain factor and then applied to the structure as an initial defect, with the defect size not exceeding 1% of the pipe's diameter. The ultimate axial bearing capacity for PVC pipe of different lengths and wall thicknesses under uniform axial loading is listed in Table 6.

Table 6. Ultimate bearing capacity of PVC pipe under axial uniform load.

| t (mm) \ L (m)	0.3	0.6	1.2	2.0	3.0	7.0
5.59	173.46	150.02	173.49	209.23	144.40	23.60
7.45	297.17	309.7	383.92	366.42	191.98	30.89
8.94	410.43	420.54	489.19	444.15	228.78	35.63
11.8	633.33	635.78	681.99	590.37	296.35	46.12
14.91	856.82	889.27	887.28	726.01	365.77	56.93
22.36	1364.97	1367.53	1378.56	1044.29	511.73	80

Figure 10a,b display the variation in the ultimate bearing capacity of PVC pipes under axial uniform force as a function of the L/D ratio and D/t ratio. The ultimate bearing capacity showed a stepped pattern of variation as the L/D ratio increased. The ultimate bearing capacity remained relatively constant with only slight fluctuations at L/D = 6. This is because deformations in the model are more likely to be influenced by boundary conditions at lower L/D ratios. However, when the L/D ratio was greater than 6, the ultimate bearing capacity gradually decreased as the L/D ratio increased. When the L/D ratio became sufficiently large, the ultimate bearing capacity of PVC pipes was no longer affected by wall thickness. The ultimate bearing capacity for PVC pipes with different wall thicknesses tended to decrease and eventually converge to similar values.
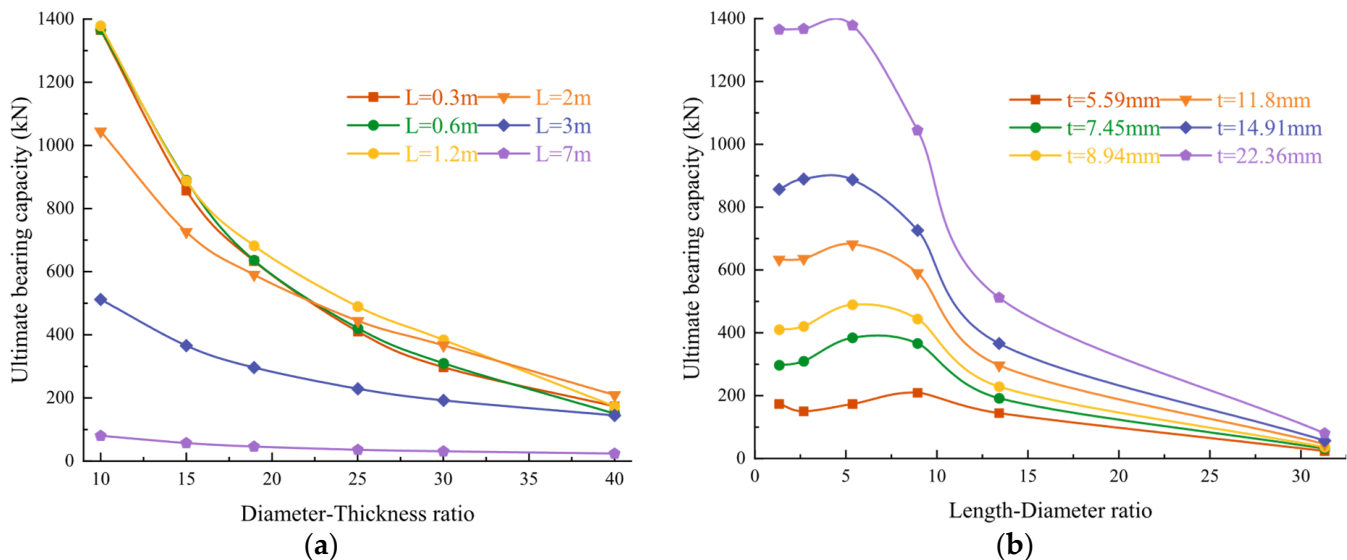
Figure 10. The curve of the ultimate bearing capacity of the pipe changing with the diameter–thickness ratio and the length–diameter ratio: (**a**) diameter–thickness ratio; (**b**) length–diameter ratio.

As can be seen from Figure 10b, the ultimate bearing capacity of PVC pipes gradually decreased as D/t increased. The ultimate bearing capacity curves of the PVC pipes with lengths of 0.3 m and 0.6 m were almost identical, and shorter pipes are more easily affected by the wall thickness ratio. For pipes with lengths of 0.3 m and 0.6 m, as the D/t ratio increased from 10 to 40, the ultimate bearing capacity decreased from 1364 kN to 173 kN—a reduction of about 1191 kN. In contrast, for a 7 m-long PVC pipe, the ultimate bearing capacity decreased from 80 kN to 23.6 kN as the D/t ratio increased from 10 to 40. This indicates that shorter pipes are significantly more affected by changes in the D/t ratio, whereas longer pipes are less influenced by these variations.

The results from Method A and Method B were compared, as shown in Figure 11. The ultimate bearing capacity of PVC pipes under axial uniform force was close to the results from Method A when the L/D ratio was less than 6. However, the difference between the ultimate bearing capacity and Method A's results increased as the L/D ratio exceeded 6. When the L/D ratio was less than 6, the ultimate bearing capacity of the pipe was primarily determined by the material's yield strength. When the L/D ratio was greater than 6, the buckling failure of the pipe was mainly governed by its axial buckling load. Zhen [14] studied the influence of the slenderness ratio of the steel pipe jacking on the critical buckling load and found that there is a critical slenderness ratio, which causes local buckling and global buckling of the steel pipe jacking. When the slenderness ratio was less than 37, local buckling occurred in the steel pipe jacking, and the critical bearing capacity was determined by the buckling load. The length of PVC pipe used in pipe jacking is shorter than that of steel pipe jacking, and the critical slenderness ratio of PVC pipe jacking is 6.
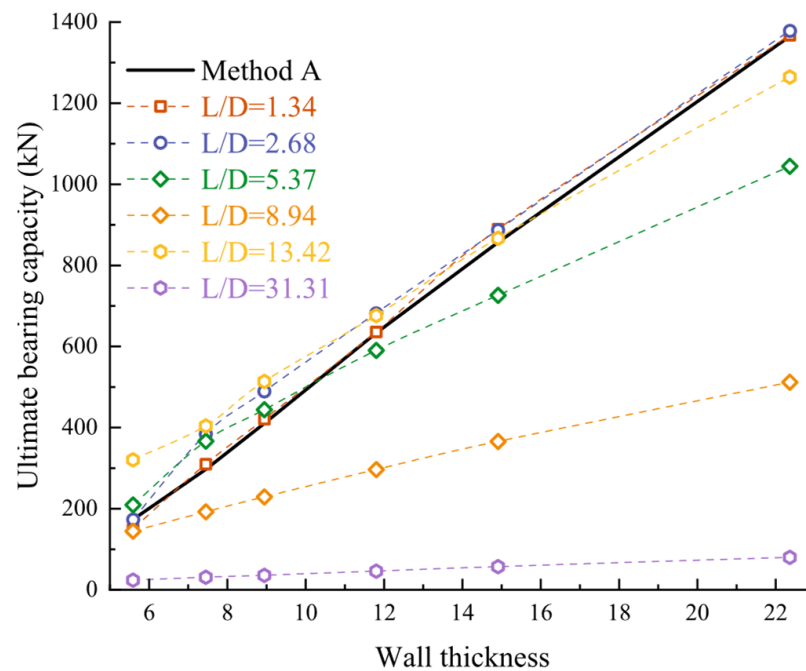
Figure 11. Comparison of results between Method A and Method B.

To compare the critical values of elastic instability with those of elastoplastic instability, the elastic buckling values from Table 5 were divided by the corresponding ultimate bearing capacity values from Table 6 to derive Table 7. As can be seen in Table 7, as the length of the pipe increased, the elastic buckling load for PVC pipe jacking gradually approached the ultimate bearing capacity under axial uniform force. When the length reached 2 m, the elastic buckling load and the ultimate bearing capacity were nearly identical. Considering the comparison between the elastic buckling results and the long pipe theory formula, it can be found that the buckling load at this time should also approach the result of the Euler compression rod theory formula.

Table 7. The ratio of elastic buckling load to ultimate bearing capacity.

t (mm) \ L (m)	0.3	0.6	1.2	2.0	3.0	7.0
5.59	0.49	0.44	0.56	0.79	0.97	0.88
7.45	0.49	0.54	0.73	0.89	0.99	1.00
8.94	0.48	0.52	0.70	0.92	0.99	0.97
11.8	0.43	0.45	0.60	0.95	1.00	0.98
14.91	0.38	0.44	0.52	0.95	1.01	0.98
22.36	0.30	0.35	0.40	0.97	1.01	1.00

4. Results under Eccentric Load

The axis deviation caused by uneven softness and improper correction of the stratum will cause the pipe to be pressed by the eccentric axis during the pipe-jacking construction. Currently, the pipe is unevenly stressed, the stability of the pipe is often reduced accordingly, and the safety of the pipe jacking structure is greatly affected. To investigate the stability of PVC pipes under eccentric axial pressure, two scenarios were analyzed in this paper:

a. Full-section radial triangular load with an eccentricity of $r/2$, as shown in Figure 12a, hereinafter referred to as L1;

b. Half-section uniformly distributed load with an eccentricity of $2r/\pi$, as shown in Figure 12b, hereinafter referred to as L2.
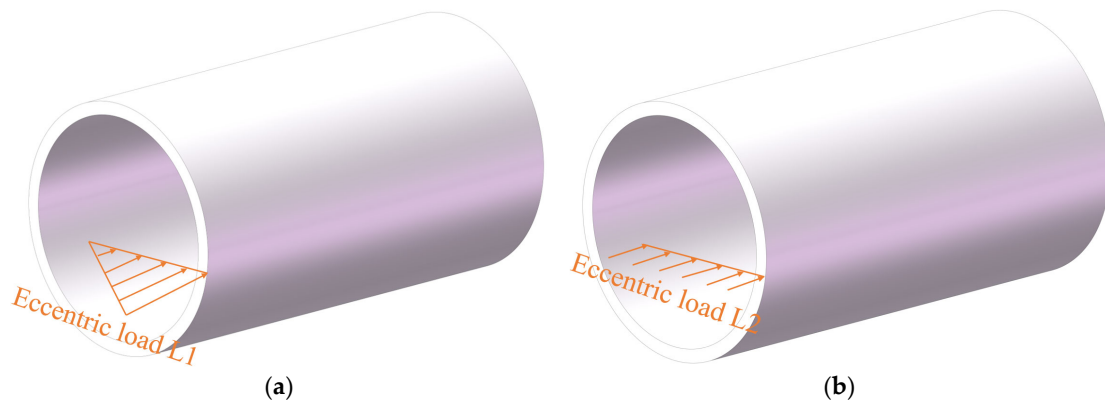
Figure 12. Schematic diagram of two types of eccentric loads: (**a**) L1 load; (**b**) L2 load.

4.1. Buckling Load of PVC Pipe

The PVC pipes were subjected to boundary conditions with one end fixed and the other hinged in the eccentric axial pressure model. Two pressurization methods were adopted: full-section radial triangular load (L1) and half-section uniformly distributed load (L2). The buckling modes for these two eccentric loading conditions of different lengths and different wall thicknesses are shown in Figures 13 and 14, respectively. The buckling modes for 3 m-long PVC pipes under the two different loading conditions are shown in Figure 15a and 15b, respectively.
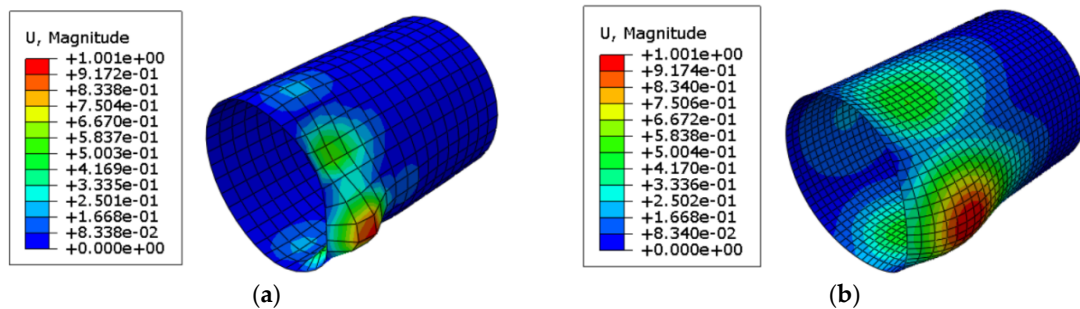

Figure 13. Buckling mode of 0.3 m pipe under L1 load: (**a**) t = 5.59 mm; (**b**) t = 22.36 mm.
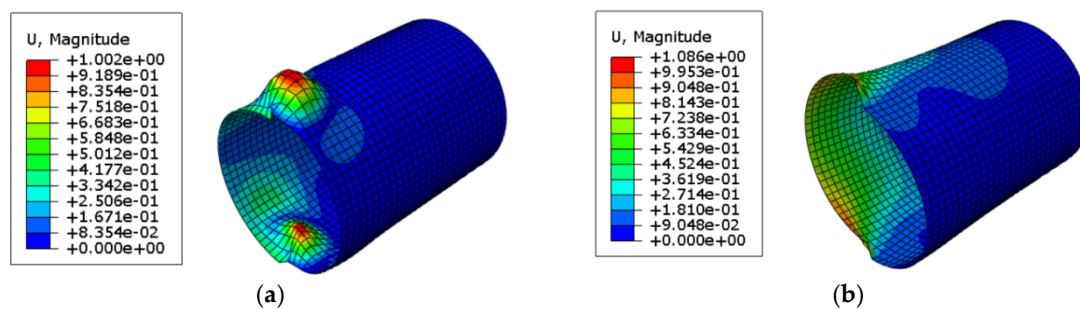

Figure 14. Buckling mode of 0.3 m pipe under L2 load: (**a**) t = 5.59 mm; (**b**) t = 22.36 mm.

Under the two eccentric loading conditions, the buckling modes of the pipes transitioned from localized failure in short pipes to an Euler buckling pattern in longer pipes as the L/D ratio increased. The number of circumferential waves also decreased in shorter pipes, and the wave peaks shifted toward the top and bottom ends of the pipe. For longer pipes, the buckling modes under both eccentric loading conditions were nearly identical to those under axial uniform force. It indicates that in this failure pattern, the impact of wall thickness on the critical buckling load can be amplified, while the impact of the length–diameter ratio may be reduced.
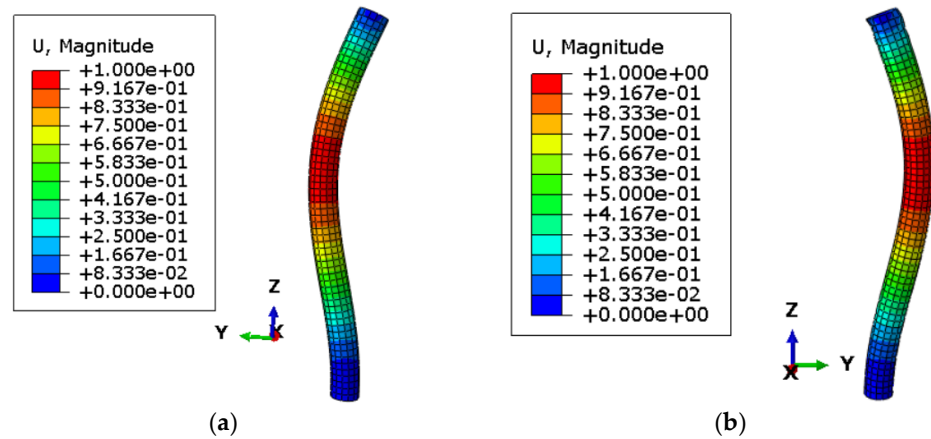
Figure 15. Buckling mode of 3 m pipe: (**a**) L1 load (**b**) L2 load.

The pipe length and thickness were changed, and the curves showing how the buckling values of PVC pipes changed with the D/t ratio and L/D ratio under two different loading conditions are depicted in Figure 16a and 16b, respectively. As seen in Figure 16a, the elastic buckling values gradually decreased with increasing D/t and L/D ratios. Additionally, the decrease in elastic buckling as the L/D ratio increased appears to be more staged. For the same diameter–thickness ratio, shorter pipes often have higher yield loads, but this trend diminished as the D/t ratio increased. At a D/t ratio of 10, the buckling load of a 0.3 m PVC pipe was 3059 kN, while the buckling load of a 7 m PVC pipe was only 80 kN, making the shorter pipe's buckling load 38 times greater. When the D/t ratio increased to 40, the difference was reduced to just 9 times. It indicates that as the pipe wall thickness decreases beyond a certain point, the influence of the length on the pipe buckling load will be gradually weakened.
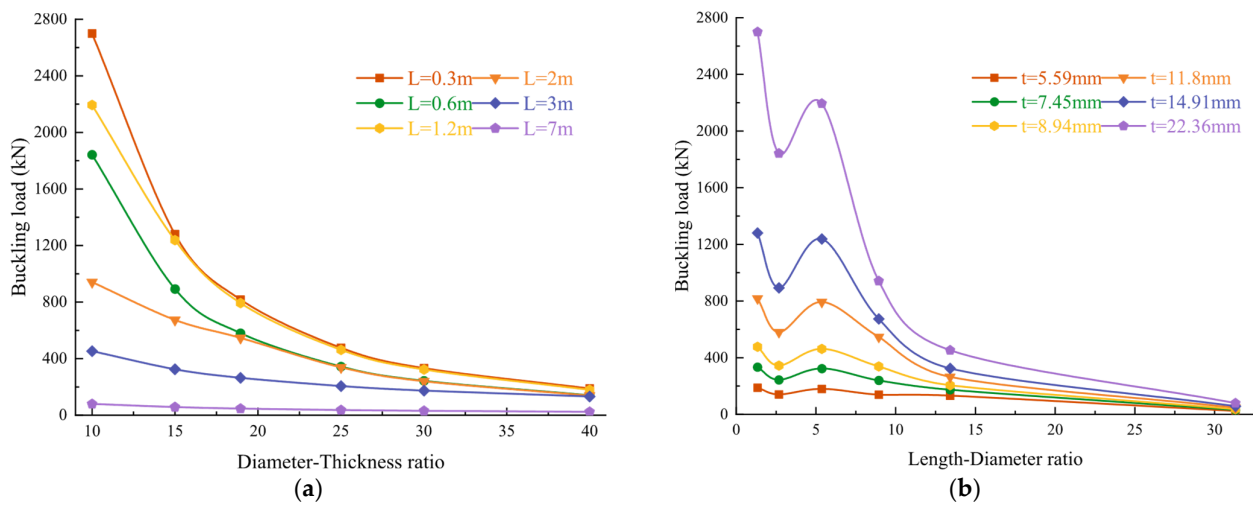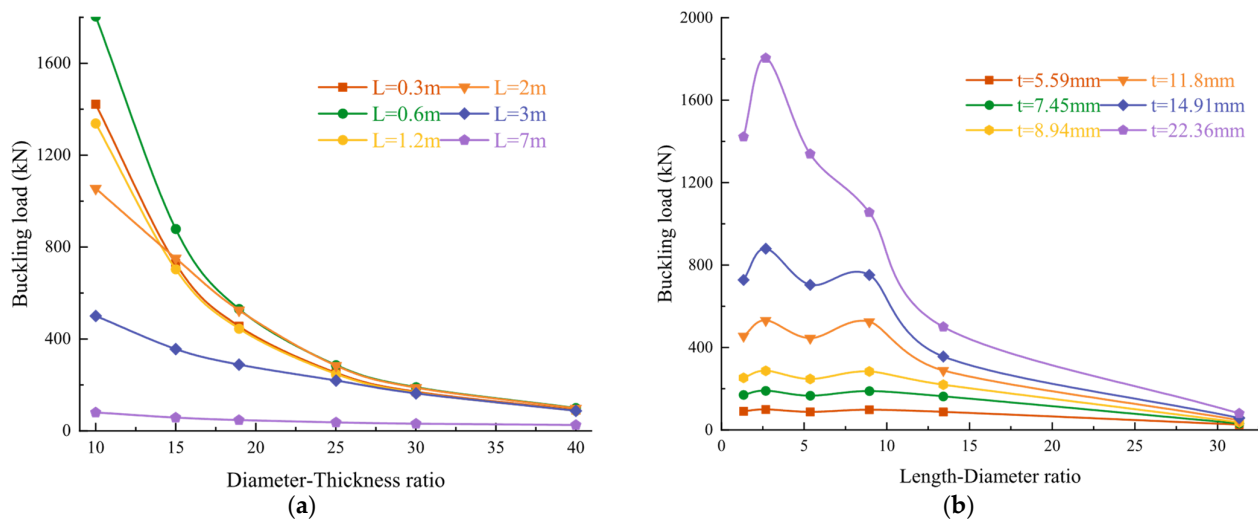

Figure 16. Variation curve of elastic buckling load with diameter–thickness ratio and length–diameter ratio under L1 load: (**a**) diameter–thickness ratio; (**b**) length–diameter ratio.

It can be observed from Figure 16b that under the action of eccentric load L1, the buckling load exhibits fluctuating variations when the L/D ratio is less than 6, with more significant fluctuations for PVC pipes with greater wall thickness. When the L/D ratio was greater than 6, the buckling load gradually decreased as the L/D ratio increased, eventually approaching zero. The main reason for this phenomenon is that the buckling modes of PVC pipes vary significantly with changes in the L/D ratio, and the critical buckling load will be affected.

Figure 17a,b exhibit the buckling load changing curves with the D/t ratio and L/D ratio under L2 load, respectively. The overall pattern was similar to that observed under the L1 load: the buckling load decreased with an increase in the D/t ratio, and the changes concerning the L/D ratio exhibited a phased pattern, with the buckling load gradually decreasing as the L/D ratio increased, particularly when L/D exceeded 6.

Figure 17. Variation curve of elastic buckling load with diameter–thickness ratio and length–diameter ratio under L2 load: (**a**) diameter–thickness ratio; (**b**) length–diameter ratio.

However, a notable difference is that the buckling loads obtained with the L2 loading form were significantly lower than those from the L1 loading form, with the maximum buckling loads differing by up to 900 kN. Furthermore, when the L/D ratio was 6, the buckling load under the L2 load first increased and then decreased, whereas under the L1 load, it first decreased and then increased. This indicates that under eccentric axial force when the pipe is shorter, the mode and magnitude of failure are strongly influenced by the type of loading and the point of load application.
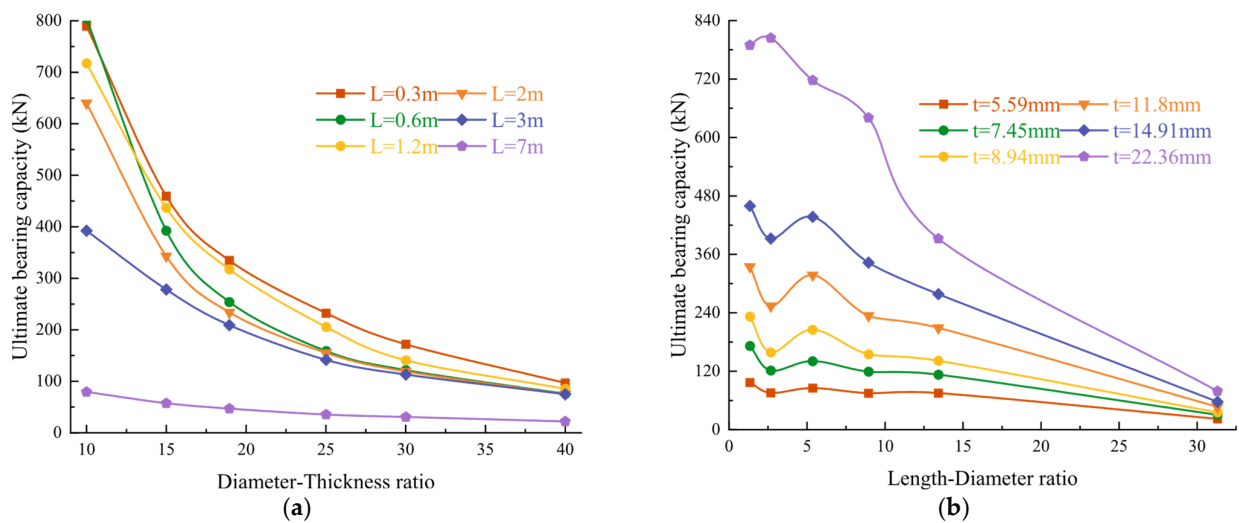
4.2. Ultimate Bearing Capacity Analysis

The ultimate bearing capacity was obtained by introducing the previously calculated elastic buckling load results into the elastoplastic buckling analysis in the same manner. The computed results are shown in Table 8. The curves depicting the ultimate bearing capacity of PVC pipe jacking under the two eccentric loadings as the length–diameter ratio and diameter–thickness ratio are shown in Figures 18 and 19, respectively.
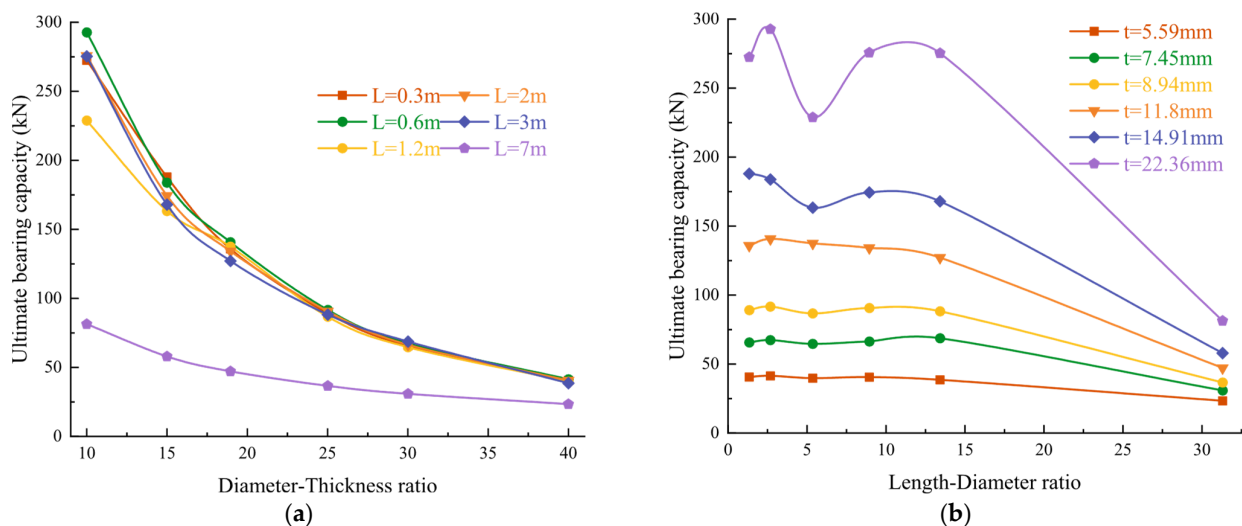
Table 8. Ultimate bearing capacity of PVC pipe under two eccentric loads.

Eccentric Load Form	L (m) t (mm)	0.3	0.6	1.2	2.0	3.0	7.0
L1	5.59	96.68	75.56	85.44	74.82	75.00	22.05
	7.45	171.81	121.50	140.74	118.97	112.90	30.49
	8.94	232.34	158.79	205.29	155.01	141.40	35.31
	11.8	334.60	253.97	317.27	233.80	208.95	46.91
	14.91	459.54	392.48	436.82	342.94	278.25	57.27
	22.36	789.55	804.28	717.45	640.23	392.23	79.13
L2	5.59	40.61	41.43	39.75	40.53	38.54	23.38
	7.45	65.64	67.33	64.57	66.40	68.64	30.82
	8.94	89.14	91.63	86.64	90.54	88.18	36.59
	11.8	135.84	140.69	137.45	134.11	127.10	47.13
	14.91	187.95	183.76	163.29	174.34	167.92	57.86
	22.36	272.44	292.72	228.76	275.72	275.33	81.32

Figure 18. Change curve of ultimate bearing capacity under L1 load: (**a**) diameter–thickness ratio; (**b**) length–diameter ratio.

Figure 19. Change curve of ultimate bearing capacity under L2 load: (**a**) diameter–thickness ratio; (**b**) length–diameter ratio.

As plotted in Figure 18a, the ultimate bearing capacity of PVC pipes gradually decreased as the D/t ratio increased, with shorter pipes being more significantly affected by changes in D/t. As D/t increased from 10 to 40, the ultimate bearing capacity of a 0.3 m-long pipe decreased by about 700 kN. It gradually decreased, and finally the ultimate bearing capacity tended to be equal. When the pipe length was between 0.3 m and 2 m, the ultimate bearing capacity of PVC pipes was not much different.

As can be seen from Figure 18b, under the L1 loading condition, the ultimate bearing capacity exhibited a staged relationship with wall thickness when the L/D ratio was less than 6. When the wall thickness was less than or equal to 14.91 mm, the numerical results first decreased and then increased with increasing L/D ratio. However, when the wall thickness was greater than 22 mm, the trend was reversed: the ultimate bearing capacity first increased and then decreased with the increasing L/D ratio. When the L/D ratio exceeded 6, the ultimate bearing capacity generally decreased as the L/D ratio increased.

Figure 19 displays the variation of the ultimate bearing capacity with the diameter–thickness ratio and length–diameter ratio under L2 eccentric load. The overall trend of the curves was consistent with that under the L1 loading condition—both decreased as

D/t and L/D increased. The ultimate bearing capacity under L2 remained at roughly the same level when L/D was greater than 14, but when L/D = 6 the ultimate bearing capacity decreased significantly, which was also mainly controlled by the change in buckling mode. The maximum ultimate bearing capacity for the pipe was only about 300 kN under the L2 loading condition, significantly lower than that under L1. Therefore, with the L2 type of eccentric loading, failure of the pipe may occur more readily, which should be noted.

To study the impact of eccentricity on the ultimate load capacity of pipes, 0.3 m-, 3 m-, and 7 m-long pipes were selected, and the ultimate bearing capacities under L1 and L2 loads were compared with those under axial uniform force. As depicted in the figure, when the pipe length was 0.3 m and 3 m, with increasing wall thickness, the ratio of the ultimate bearing capacity under L1 and L2 loads to that under axial uniform force tended to stabilize. It can be seen from Figure 20 that with an eccentricity of 0.5, corresponding to the L1 load, the ultimate bearing capacity was about 55% of that under axial uniform force. With an eccentricity of 0.6366, representing the L2 load, the ultimate bearing capacity was approximately 22% of the capacity under axial uniform force.
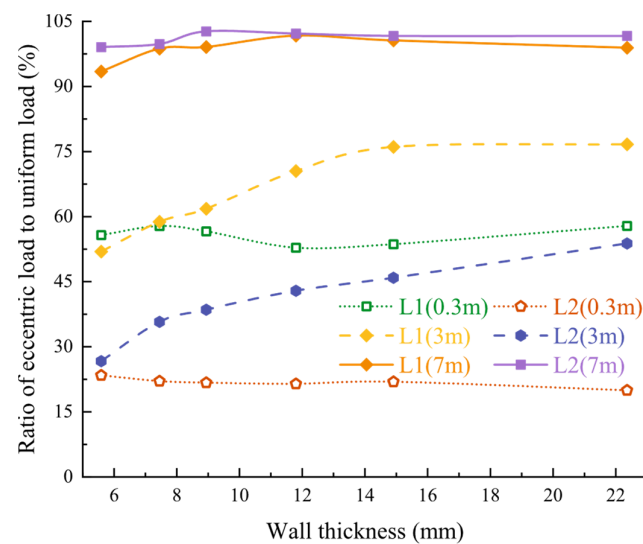
Figure 20. The ratio of ultimate bearing capacity under eccentric load and uniform load for different pipe lengths.

When the length of the pipe increased to 3 m, the proportion of L1 and L2 to the uniform load increased from 55% to about 80% and 22% to about 50%, respectively, both of which are significantly improved. It was found that with the increase of the L/D ratio, the influence of the load distribution form on the ultimate bearing capacity gradually decreased, and the ultimate bearing capacity under the two eccentric loads continued to rise. Moreover, at lower L/D ratios, loads with higher eccentricity led to a greater reduction in the ultimate bearing capacity of the pipes. However, when the pipe length increased to 7 m, the ratio of the ultimate bearing capacity of the two eccentric loads to the uniform axial compression was almost the same, both of which were about 100%, indicating that the ultimate bearing capacity under L1 and L2 loads was almost the same as that under uniform axial compression.

The relationship between the bearing capacity under two types of eccentric loading and the length–diameter ratio was compared. The greater impact of initial defects when the wall thickness was smaller was considered, and a thickness of t = 22.36 mm was chosen. The comparison results are shown in Figure 21. For L/D ratios ≤ 6, the buckling mode exhibited localized failure, and the bearing capacity should primarily be influenced by the failure mode and material strength. The ratios of L1 and L2 to the uniform load were maximized at around 22% and 60%, respectively.
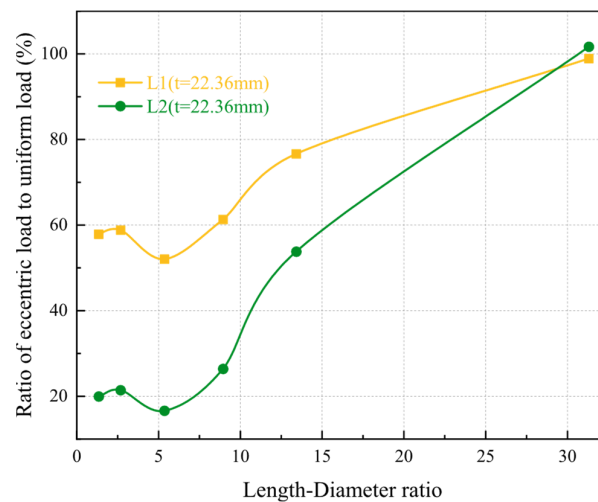
Figure 21. Ratio of ultimate bearing capacity under two eccentric loads and uniform load.

At L/D greater than 6, the buckling mode of the pipe gradually transitioned to Euler buckling with increasing length–diameter ratio. However, the development of the buckling mode under uniform loading and different eccentric loadings varied during the process of increasing the length–diameter ratio. Overall, the ratio of the ultimate bearing capacity under both types of eccentric loading to the ultimate bearing capacity under uniform loading increased continuously with an increasing L/D ratio. When L/D reached 30, it tended to be consistent with the ultimate bearing capacity under uniform loading.

5. Discussion

When PVC pipe jacking is subjected to axial pressure, material failure may occur first or buckling may occur first according to the numerical analysis above. Under axial uniform force when L/D $\leq$ 6, PVC pipes are prone to experience yield failure first, the magnitude of which is determined by the yield strength of the pipe material. When L/D is greater than 6, the pipe is likely to experience buckling instability first, the magnitude of which is determined by the axial buckling value of the structure.

When L/D is less than or equal to 6, the ultimate bearing capacity is $F_d = A_p \sigma_u$

$$F_p - F_0 \leq F_d = A_p \sigma_u \tag{5}$$

The allowable jacking distance L is calculated according to Equation (6).

$$L \leq \frac{A_p \sigma_{\mathrm{u}}}{\mu(N + W)} \tag{6}$$

In the formula, F_p is the allowed thrust force; F_0 is the resistance faced; A_p is the pipe cross-sectional area, m^2; σ_u is the yield strength of the pipe material, Pa; μ is the friction coefficient; N is the pipe pressure; and W is the pipe gravity.

In the range of $6 < $ L/D ≤ 8.5, the ultimate bearing capacity of the pipe is less than the theoretical value of full-section yielding. The finite element analysis method can be used to analyze its buckling type and determine its critical buckling load to accurately calculate its ultimate bearing capacity.

When L/D is greater than 8.5, the ultimate bearing capacity depends on its axial buckling value. At this point, the ultimate bearing capacity of the pipe is close to the elastic buckling value, thus exhibiting good consistency with the Euler formula for long pipes.

$$F_p - F_0 \leq F_d = \frac{\pi^3 E D^3 t}{8(\mu_0 l)^2} \tag{7}$$

$$L \leq \frac{\pi^3 E D^3 t}{8\mu(N+W)(\mu_0 l)^2} \tag{8}$$

According to the CECS-2020 [31], the maximum allowable jacking force of the dowel surface for pipe jacking is calculated according to the following Formula (9). In the design process of pipe jacking engineering, it is slightly conservative to select the value of pipe–soil friction resistance according to the current standard specification. The relationship between the change of the length–diameter ratio and the buckling of the pipeline is considered in this paper. The allowable jacking force and jacking distance derived from different length–diameter ratios are more applicable.

$$F_d = K_d \frac{f_p A_p}{\gamma_d \times 10^3} \tag{9}$$

$$f_p = \frac{f_{p,k}}{\gamma_c} \tag{10}$$

In the formula, K_d is the eccentric compression allowing the jacking force reduction factor. γ_d is the allowable jacking force comprehensive coefficient, and the value of the PVC pipe is 1.11. $f_{p,k}$ is the standard value of axial compressive strength of the pipe, and the value of the PVC pipe is 66 MPa. γ_c is the partial coefficient of axial compressive strength, and the value of the PVC pipe is 1.2.

Under the eccentric axial pressure L1, the short pipe exhibits asymmetric local buckling along the axial direction. Based on the comparative analysis with axial uniform force, the ratio of the ultimate bearing capacity of L1 to that of axial uniform force fluctuates around a certain value at L/D ≤ 6, with this ratio varying with the wall thickness, generally around 50%. For 6 < L/D < 30, the ultimate bearing capacity of L1 gradually approaches that of axial uniform force with the increase of L/D. For accurate calculation, finite element analysis methods can be employed. When 30 ≤ L/D, the ultimate bearing capacity of L1 approaches that of axial uniform force, calculated according to Equation (7).

Under the eccentric axial pressure L2, when L/D ≤ 14, the ultimate bearing capacity of the pipe fluctuates around a certain value as a whole; when 14 < L/D < 30, the ultimate bearing capacity under L2 increases with the length–diameter ratio. The increase gradually approaches the ultimate bearing capacity under axial uniform force. If you want to calculate accurately, you can use the finite element analysis method; when 30 ≤ L/D, the ultimate bearing capacity is calculated using Equation (7).

PVC pipes typically have outer diameters ranging from 200 to 600 mm and lengths of around 1 m in micro tunneling. When only the axial uniform force is considered, when the pipe diameter is greater than 333 mm, the yield strength of the pipe is mainly considered. However, for pipe diameters ranging from 200 to 333 mm, a specific analysis needs to be conducted in conjunction with the pipe length.

6. Conclusions

The failure forms and buckling modes of PVC pipes under uniform and eccentric loads were investigated, and the buckling load and ultimate bearing capacity at different length–diameter ratios and diameter-thickness ratios were obtained through theoretical research and numerical simulation. The key conclusions were drawn as follows:

(a) The elastic buckling load of PVC pipes decreases continuously with an increasing length–diameter ratio and diameter–thickness ratio under axial uniform force. It closely approximates the short pipe theory formula when L/D is less than or equal to 6 and tends to approach the long pipe theory formula when L/D exceeds 8.5. The elastic-plastic buckling is calculated by introducing an initial defect, and the ultimate bearing capacity of the pipe is obtained. When the L/D ratio is less than or equal to 6, the ultimate bearing capacity of the pipe tends to approach the theoretical yield failure value. When L/D is greater than 6, the pipe buckles and becomes unstable, and its magnitude is determined by the axial buckling value of the structure.

(b) The mode of failure and the magnitude of the buckling load of the pipe are significantly influenced by the manner and location of the loading under eccentric axial loading. Short pipes exhibit asymmetric local failures under eccentric loading, gradually transitioning to Euler buckling modes as the length–diameter ratio increases. The buckling load of the pipe under eccentric axial loading is notably lower than that under axial uniform force. However, as the length–diameter ratio increases, the difference between the two decreases, indicating that the influence of the loading mode and distribution diminishes with an increasing length–diameter ratio.

(c) Based on the consideration of the load capacity of a single pipe and the relationship between the ultimate bearing capacity of the pipe under different L/D ratios and the fourth yield criterion and Euler's formula, the calculation methods of allowable jacking force and single allowable jacking distance is derived.

(d) To prevent PVC pipes from buckling during jacking, when the length–diameter ratio is less than 6, priority should be given to the yield failure of the pipe. When the length–diameter ratio is greater than 6, priority should be given to the axial buckling value of the pipe under a certain length–diameter ratio of the pipe. The increase in wall thickness can increase the strength failure value and the axial buckling failure value of the pipe. However, it also increases the production cost of the pipe. Therefore, the wall thickness of the pipe should be determined based on the permissible jacking force.

However, there are still limitations in the FEM and results that can be further investigated. In the simulation, the soil–structure interaction (SSI) is not considered. The frictional resistance is derived from soil pressure acting on the pipe and the shear behavior of the SSI. The uncertainty of soil parameters has a significant effect on the structure [32]. The frictional resistance is also affected by soil properties and tends to be higher in dense or cohesive soils. The excessive frictional resistance induced by soil pressure increases the total jacking force and decreases the allowable jacking distance in a practical jacking drive since the critical buckling load decreases with the increase in pipe length, and the pipe is more prone to buckle under the action of jacking force. Meanwhile, the pipe jacking project is also affected by soil deformation [33,34]. The settlement of the pipe induced by the soil movement in long-distance pipe jacking will cause a deviation of the pipe axis, resulting in additional eccentricity and reduced critical buckling load and ultimate bearing capacity. Furthermore, the earth pressure generated by the SSI causes extrusion and contact with the pipes and may lead to the deformation of the pipe, resulting in a decrease in the buckling confining pressure, and the buckling of the pipe will occur under a relatively small jacking force [16].

Data Availability Statement: All data that support the findings of this study are available from the corresponding author upon reasonable request.

Conflicts of Interest: The authors declare no conflicts of interest.

References

1. Ma, B.; Najafi, M. Development and applications of trenchless technology in China. *Tunn. Undergr. Space Technol.* **2008**, *23*, 476–480. [CrossRef]
2. Zhang, P.; Behbahani, S.S.; Ma, B.; Iseley, T.; Tan, L. A jacking force study of curved steel pipe roof in Gongbei tunnel: Calculation review and monitoring data analysis. *Tunn. Undergr. Space Technol.* **2018**, *72*, 305–322. [CrossRef]

3.   Liu, K.; Ariaratnam, S.T.; Zhang, P.; Chen, X.; Wang, J.; Ma, B.; Zhang, Y.; Feng, X.; Xu, T. Mechanical response of diaphragm wall supporting deep launch shaft induced by braced excavation and pipe jacking operation. *Tunn. Undergr. Space Technol.* **2023**, *134*, 104998. [CrossRef]

4.   Liu, K.; Xiao, A.; Zhang, P.; Zhou, H.; Chen, Z.; Xu, T.; Ma, B.; Ai, H.; Wang, Q. Study on mechanical response of steel pipe jacking considering the effect of pipe sticking. *Tunn. Undergr. Space Technol.* **2022**, *127*, 104617. [CrossRef]

5.   Ji, X.; Ni, P.; Barla, M. Analysis of jacking forces during pipe jacking in granular materials using particle methods. *Undergr. Space* **2019**, *4*, 277–288. [CrossRef]

6.   Li, C.; Zhong, Z.; Bie, C.; Liu, X. Field performance of large section concrete pipes cracking during jacking in Chongqing—A case study. *Tunn. Undergr. Space Technol.* **2018**, *82*, 568–583. [CrossRef]

7.   Zhang, P.; Feng, X.; Zeng, C.; Ariaratnam, S.T. Field performance of steel pipes during curve jacking in Gongbei tunnel. *Tunn. Undergr. Space Technol.* **2022**, *128*, 104585. [CrossRef]

8.   Najafi, M.; Iseley, D.T. Evaluation of PVC Pipe for Microtunneling. In *Buried Plastic Pipe Technology: 2nd Volume*; ASTM Special Technical Publication; ASTM: West Conshohocken, PA, USA, 1994; Volume 1222, p. 220.

9.   Chapman, D.N.; Rogers, C.D.F.; Burd, H.J.; Norris, P.M.; Milligan, G.W.E. Research needs for new construction using trenchless technologies. *Tunn. Undergr. Space Technol.* **2007**, *22*, 491–502. [CrossRef]

10. Ryan, P.K.; Finney, A.J. Pipe materials and joint selection for trenchless construction. In Proceedings of the Pipelines 2012: Innovations in Design, Construction, Operations, and Maintenance, Doing More with Less 2012, Miami Beach, FL, USA, 19–22 August 2012; pp. 928–939.

11. Kramer, S.R.; McDonald, W.J.; Thomson, J.C.; Kramer, S.R.; McDonald, W.J.; Thomson, J.C. Pipe jacking and microtunnelling. In *An Introduction to Trenchless Technology*; Springer: Berlin/Heidelberg, Germany, 1992; pp. 86–120.

12. Jemii, H.; Bahri, A.; Boubakri, A.; Hammiche, D.; Elleuch, K.; Guermazi, N. On the mechanical behaviour of industrial PVC pipes under pressure loading: Experimental and numerical studies. *J. Polym. Res.* **2020**, *27*, 240. [CrossRef]

13. Tang, P.; Hu, S.; Liu, G.; Ye, Y.; Pan, F.; Hou, Z. Mechanical Properties and Structural Optimization Analysis of PVC Axial Hollow-wall Pipe for Drainage. *Adv. Eng. Sci.* **2023**, 1–11. (In Chinese) [CrossRef]

14. Zhen, L.; Qiao, P.; Zhong, J.; Chen, Q.; Chen, J.J.; Wang, J. Design of steel pipe-jacking based on buckling analysis by finite strip method. *Eng. Struct.* **2017**, *132*, 139–151. [CrossRef]

15. Wang, Y.; Qiao, P.; Lu, L. Buckling analysis of steel jacking pipes embedded in elastic tensionless foundation based on spline finite strip method. *Thin-Walled Struct.* **2018**, *130*, 449–457. [CrossRef]

16. Zhen, L.; Chen, J.-J.; Qiao, P.; Wang, J.-H. Analysis and remedial treatment of a steel pipe-jacking accident in complex underground environment. *Eng. Struct.* **2014**, *59*, 210–219. [CrossRef]

17. Fok, S.L. Analysis of the buckling of long cylindrical shells embedded in an elastic medium using the energy method. *J. Strain Anal. Eng. Des.* **2002**, *37*, 375–383. [CrossRef]

18. Tu, S.; Shuai, J. Numerical study on the buckling of pressurized pipe under eccentric axial compression. *Thin-Walled Struct.* **2020**, *147*, 106542. [CrossRef]

19. Huang, C.; Chen, J.; Sun, Y. Mechanical simulation and calculation methodology of buried steel pipes under multiple loads. *Case Stud. Constr. Mater.* **2022**, *17*, e01662. [CrossRef]

20. Alotaibi, E.; Omar, M.; Shanableh, A.; Zeiada, W.; Fattah, M.Y.; Tahmaz, A.; Arab, M.G. Geogrid bridging over existing shallow flexible PVC buried pipe–Experimental study. *Tunn. Undergr. Space Technol.* **2021**, *113*, 103945. [CrossRef]

21. Costa, Y.D.; Zornberg, J.G.; Costa, C.M. Physical modeling of buried PVC pipes overlying localized ground sub-sidence. *Acta Geotech.* **2021**, *16*, 807–825. [CrossRef]

22. Mei, Z.; Xiao, A.; Mei, J.; Hu, J.; Zhang, P. Experimental Study on Interface Frictional Characteristics between Sand and Steel Pipe Jacking. *Appl. Sci.* **2023**, *13*, 2016. [CrossRef]

23. Hu, Q.; Li, X.; Han, X.; Li, H.; Chen, J. A normalized stress invariant-based yield criterion: Modeling and validation. *Int. J. Plast.* **2017**, *99*, 248–273. [CrossRef]

24. Małachowski, E.; L'vov, G.; Daryazadeh, S. Numerical prediction of the parameters of a yield criterion for fibrous composites. *Mech. Compos. Mater.* **2017**, *53*, 589–600. [CrossRef]

25. Fajuyitan, O.K.; Sadowski, A.J.; Wadee, M.A.; Rotter, J.M. Nonlinear behaviour of short elastic cylindrical shells under global bending. *Thin-Walled Struct.* **2018**, *124*, 574–587. [CrossRef]

26. Luo, Z.; Zhu, Y.P.; Zhao, X.Y.; Wang, D.Y. Hi28gh-order vibrations' dynamic scaling laws of distorted scaled models of thin-walled short cylindrical shells. *Mech. Based Des. Struct. Mach.* **2015**, *43*, 514–534. [CrossRef]

27. Farshidianfar, A.; Farshidianfar, M.H.; Crocker, M.J.; Smith, W.O. Vibration analysis of long cylindrical shells using acoustical excitation. *J. Sound Vib.* **2011**, *330*, 3381–3399. [CrossRef]

28. Saad, N.A.; Al-Maamory, M.H.; Mohammed, M.R.; Hashim, A.A. The effect of several service and weathering parameters on tensile properties of PVC pipe materials. *Mater. Sci. Appl.* **2012**, *3*, 784–792. [CrossRef]

29. Burn, S.; Davis, P.; Schiller, T.L. *Long-Term Performance Prediction for PVC Pipes*; AWWA Research Foundation: Denver, CO, USA, 2006.

30. Baysal, E.; Koçar, O.; Anaç, N.; Darıcı, F. Eşit Kanallı Açısal Presleme Yönteminde Kanal Açılarının ve İç Köşe Ka-visinin Deformasyona Etkisinin Sonlu Elemanlar Metodu ile İncelenmesi. *Çukurova Üniv. Mühendis. Fak. Derg.* **2023**, *38*, 859–873. [CrossRef]

31. *CECS246-2020*; Technical Specification for Pipe Jacking of Water Supply and Sewerage Engineering. China Engineering Construction Association, CECS: Beijing, China, 2020. (In Chinese)

32. Mina, D.; Forcellini, D. Soil–structure interaction assessment of the 23 November 1980 Irpinia-Basilicata earthquake. *Geosciences* **2020**, *10*, 152. [CrossRef]

33. Rajeev, P.; Tesfamariam, S. Seismic fragilities of non-ductile reinforced concrete frames with consideration of soil structure interaction. *Soil Dyn. Earthq. Eng.* **2012**, *40*, 78–86. [CrossRef]

34. Rathje, E.; Pehlivan, M.; Gilbert, R.; Rodriguez-Marek, A. Incorporating site response into seismic hazard assessments for critical facilities: A probabilistic approach. In *Perspectives on Earthquake Geotechnical Engineering: In Honour of Prof. Kenji Ishihara*; Springer: Berlin/Heidelberg, Germany, 2015; pp. 93–111.